Optimization Simulation of Temperature Control Systems for Smart Water Heaters

Xixian Xue*

1Department of School of Automation Science and Engineering, Xi'an Jiaotong University, Xi'an, 710049, China

*Corresponding author: 286764340@stu.xjtu.edu.cn

Abstract. Cutting energy use and emissions is now central to social progress, and buildings have become a primary target. Smart-home technology can meet individual comfort demands while trimming consumption. Yet today's installations still waste power and their subsystems rarely coordinate. This paper examines a coupled controller that links air-conditioning with a domestic water heater. A thermodynamic model drives an automation layer that diverts part of the air conditioner's rejected heat to pre-warm the tank. Dynamic simulations and energy accounting show the two loops are tightly coupled: room-temperature control remains robust when its own set-point changes, whereas hot-water regulation is easily disturbed by the air conditioner's operating state. The runs also chart a clear downward trend in overall demand. Overlaying room and water temperature transients confirms that the recovered heat yields both significant and replicable sizeable savings. The scheme is readily packaged for commercial products and offers manufacturers a route to upgrade their lines to quickly implement.

Keywords: Smart home automation; energy conservation; temperature control; Proportional-Integral-Derivative (PID).

1. Introduction

Global energy demand keeps climbing, and the push for carbon peaking and neutrality has made cutting energy use and emissions a central task. Among the three largest energy-consuming sectors, construction stands out: operating buildings now claims roughly 30% of final energy worldwide, with heating, ventilation and air-conditioning alone responsible for about 60% of that share [1-5]. Market pulls and policy incentives are widening the reach of smart-home solutions. Cheaper, more reliable Internet of Things (IoT) and sensor hardware has cleared the way for mass adoption; Kinect-type devices, for instance, can track user-defined poses or gestures and translate them directly into control commands [6]. Heat pumps and heat-recovery ventilators give households fresh options for cascading energy use and lifting overall efficiency. Industrial practice shows that modeling and system identification usually consume the greatest share of time and budget in any research program [7, 8]. The control layer governs Heating, Ventilation and Air Conditioning (HVAC) reliability: it balances thermal comfort against energy use and now extends beyond simple load shaving to demand response and the absorption of on-site renewables [9]. The central design problem is therefore to curb, or productively reuse while preserving comfort and simultaneously holding down the energy needed for domestic hot water.

Against this backdrop, developing a smart-home environmental controller that blends advanced algorithms, energy recovery and user-habit learning follows current technological momentum and offers clear prospects for saving energy and cutting emissions [4]. Conventional residential temperature regulation still relies on simple on-off loops. While cheap, this approach forces the equipment to cycle repeatedly, raising energy use, widening room-temperature swings and shortening service life [10]. The present work introduces an upgraded heat-recovery transfer controller that couples air-conditioner and water-heater loops, turning the air-conditioner's rejected heat into hot water. Feasibility and performance will first be examined through modelling and simulation. Comparative analysis and quantitative energy accounting will then measure the savings delivered by the heat-recovery technique and test the control system's robustness. Ultimately, the study seeks to supply fresh design insight for efficient, comfortable smart-home systems. The same architecture could later scale to industrial plant, allowing wider heat recovery and reuse in the global effort to curb energy demand and emissions.

2. System Principles and System Models

2.1. System Principles

The study begins by constructing a physical model of the water-heater assembly, centered on an electrically boosted tank of the kind commonly paired with solar thermal installations. Water is first warmed in a pre-heat store, picking up heat delivered from the collector loop by either air or water. It then passes to the electric unit, where its temperature is lifted to the required set-point. Inside the tank, heat transfer is governed by two coupled processes: exchange between the water and the tank walls, and losses from the outer surface to the surroundings. The variables that describe each mechanism are listed in Table 1.

Table 1. The physical meanings corresponding to the thermodynamic modeling symbols

Symbol	Physical meanings
$T_w(t)(℃)$	temperature of water
$C_w(J/℃)$	heat capacity of water
$T_t(t)(℃)$	temperature of the tank wall
$C_t(J/℃)$	heat capacity of the tank wall
$P_{in}(t)(W)$	heater power
$R_1(℃/W)$	thermal resistance between water and the tank wall
$R_2(℃/W)$	thermal resistance between the water tank wall and the external environment
$T_\infty(℃)$	Ambient temperature

Applying the conservation of energy to each storage medium (water and tank wall) yields component wise balances. For the water, the rate of energy change equals the net heat flow in minus that leaving, giving the first differential equation (1):

$$C_w \frac{dT_w}{dt} = P_{in}(t) - \frac{1}{R_1}\big(T_w(t) - T_t(t)\big) \tag{1}$$

For the water tank wall, energy change in the tank wall per unit time equals heat entering minus heat leaving, this yields the second differential equation (2):

$$C_t \frac{dT_t}{dt} = \frac{1}{R_1}\big(T_w(t) - T_t(t)\big) - \frac{1}{R_2}(T_t(t) - T_\infty) \tag{2}$$

The analysis yields a coupled system of linear second-order differential equations (3):

$$\begin{cases} C_w \frac{dT_w}{dt} = P_{in}(t) - \frac{1}{R_1}\big(T_w(t) - T_t(t)\big) \\ C_t \frac{dT_t}{dt} = \frac{1}{R_1}\big(T_w(t) - T_t(t)\big) - \frac{1}{R_2}(T_t(t) - T_\infty) \end{cases} \tag{3}$$

The Laplace transform equation (4) is performed near the steady-state operating point:

$$\theta_w(s) = \mathcal{L}[T_w(t)], \theta_t(s) = \mathcal{L}[T_t(t)], P_{in}(s) = \mathcal{L}[P_{in}(t)] \tag{4}$$

Perform a Laplace transform on the system of equations (5) (considering zero initial conditions):

$$\begin{cases} C_w s\theta_w(s) = P_{in}(s) - \frac{1}{R_1}\big(\theta_w(s) - \theta_t(s)\big) \\ C_t s\theta_t(s) = \frac{1}{R_1}\big(\theta_w(s) - \theta_t(s)\big) - \frac{1}{R_2}\big(\theta_t(s)\big) \end{cases} \tag{5}$$

Rewrite the system of equations (6) in standard form:

$$\begin{cases} \left(C_w s + \frac{1}{R_1}\right)\theta_w(s) - \frac{1}{R_1}\theta_t(s) = P_{in}(s) \\ -\frac{1}{R_1}\theta_w(s) + \left(C_t s + \frac{1}{R_1} + \frac{1}{R_2}\right)\theta_t(s) = 0 \end{cases} \quad (6)$$

By combining and simplifying the two equations, after finding a common denominator and simplifying, they can ultimately be transformed into the following equation (7):

$$G(s) = \frac{\theta_w(s)}{P_{in}(s)} = \frac{K}{(\tau_1 s+1)(\tau_2 s+1)} \quad (7)$$

The system therefore behaves as a second-order thermodynamic model, since it contains two independent energy-storage elements. Its governing differential equation inherits this order directly from the count of such components.

Indoor temperature behaves much like the temperature of a water tank. A single room exchanges heat through several boundaries: the floor couples it to the ground, while walls and windows link it to the outdoors and to neighboring rooms. To predict how the room temperature changes, every heat flow must be accounted for HVAC supply, solar gains, plug loads, and the heat emitted by occupants all add to the thermal balance [11]. For simplicity, the remaining, less-dominant effects are lumped into an additional time constant, giving the room a transfer function analogous to that of the tank. The resulting controlled-object model is summarized below:

Room temperature second order model is shown in the equation (8):

$$G_{room}(s) = \frac{T_{room}(s)}{V_{air}(s)} = \frac{K_1}{(\tau_{1a} s+1)(\tau_{1b} s+1)} \quad (8)$$

Water tank temperature second order model is shown in the equation (9):

$$G_{tank}(s) = \frac{T_{tank}(s)}{Q_{recycle}(s)} = \frac{K_2}{(\tau_{2a} s+1)(\tau_{2b} s+1)} \quad (9)$$

When the heating power steps up, the water temperature does not trace a simple first-order response; instead, it climbs slowly at first and then flattens out. The heat is initially stored in the water, conducted to the tank walls to warm them, and finally lost from the walls until equilibrium is reached.

2.2. Simulation Model of Intelligent Temperature Control System

The control law is a straightforward Proportional-Integral-Derivative (PID) algorithm: it is easy to code and has a long record of industrial use, so it was adopted here. $G_{room}(s)$ An operator enters the target temperature through the input panel, PID loops are particularly convenient for keeping the stored water in an electric heater at this set-point [12]. A coupling block captures how air-conditioner reject heat contributes to water heating; for a first approximation the conversion efficiency is treated as the linear function. Two on-screen scopes display and log the computed water and room temperatures; the resulting waveforms are exported to MATLAB, merged, and plotted on one axis. The overall sequence is summarized in Figure 1.

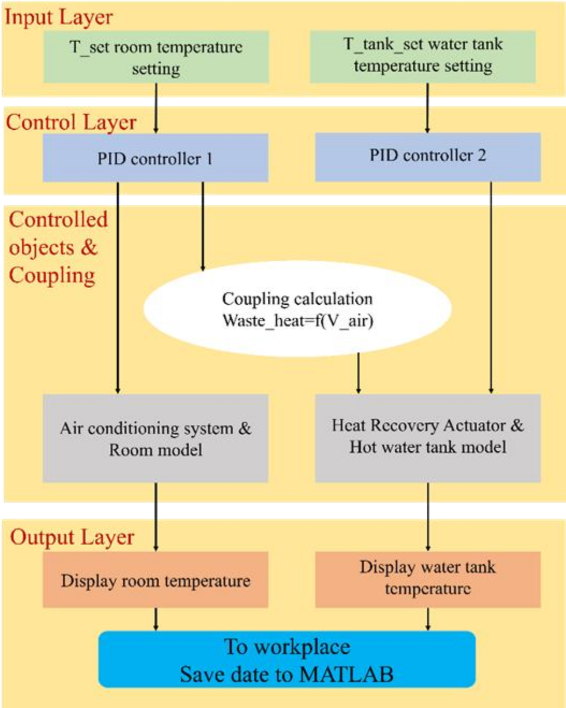

Fig. 1 Smart temperature control system flowchart (Picture credit: Original)

To anchor the comparison, the experiment is run twice: once with the heat-recovery loop active and once with it disabled as the baseline. After both simulations finish, the data are written to the MATLAB workspace, ready for scripted analysis, quantification and plotting. The full flowchart of the second configuration appears in Figure 2.

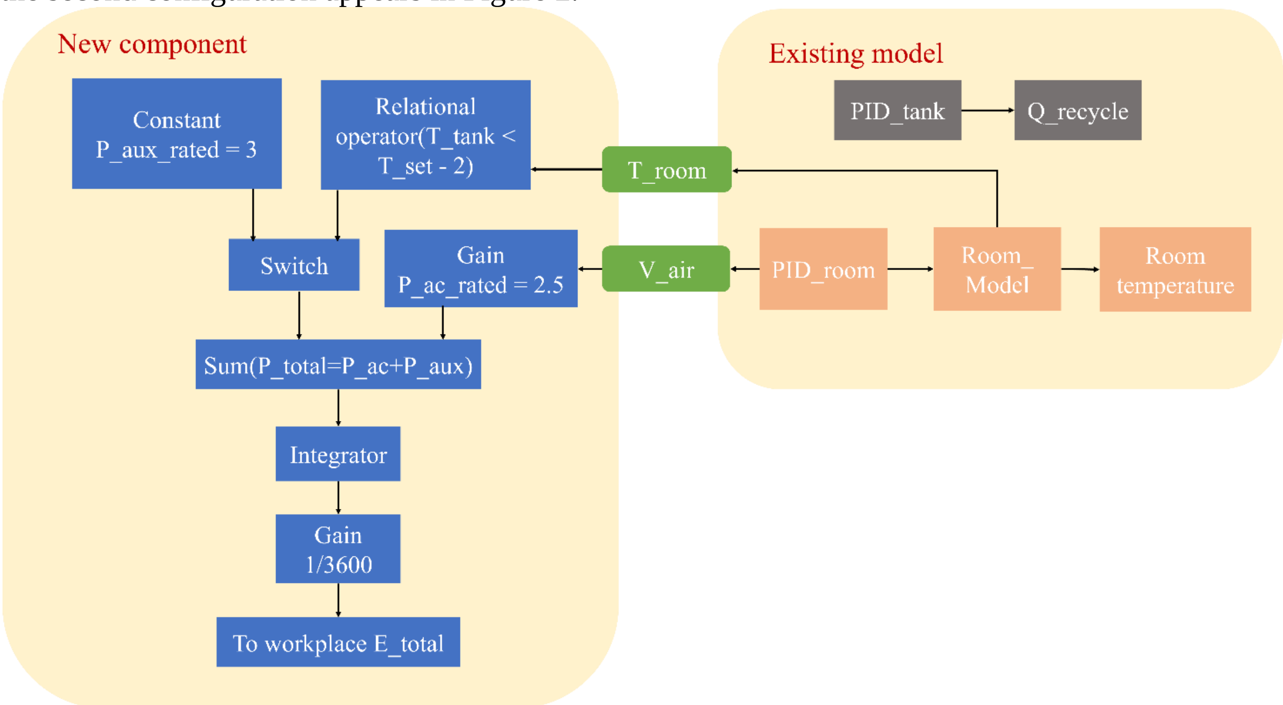

Fig. 2 Smart temperature control system energy consumption analysis flowchart (Picture credit: Original)

Sensor data collected in the field is never perfect, noise and lag creep in during both measurement and actuation. Temperature loops, in particular, suffer from sensor, communication and actuator delays. Capturing these variable lags in the model is therefore essential if the design is to reflect real world constraints. To mimic the random disturbances that appear on any plant floor, white noise has also been injected into the simulations.

The temperature-control loop was built and tested in Simulink, as shown in Figure 3. Yet the classical PID law, once its gains are fixed at commissioning, cannot keep the loop at peak performance when the environment drifts—external temperature swings or unmodelled disturbances appear. Because the parameters stay constant, the response deteriorates: overshoot grows, settling stretches, and steady-state accuracy drops.

To meet the detection and quantification goals, the simulation's system architecture must be revised. This calls for an update to the coupling function, which presently treats heat-recovery efficiency as a fixed 0.7, whereas real operation follows far more intricate thermal behavior. Before energy use can be quantified, a Gain block is inserted to define or estimate each component's instantaneous power; an Integrator block then accumulates this signal over time to yield total energy consumption.

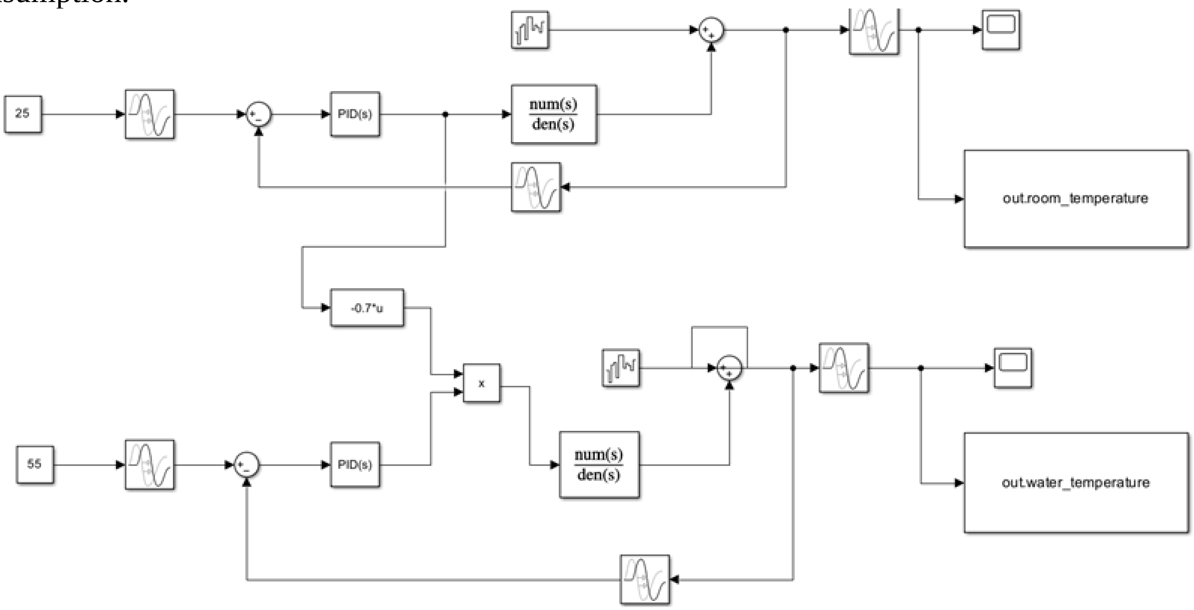

Fig. 3 Simulink model diagram for temperature control system (Picture credit: Original)

3. Results

3.1. Analysis of Room Temperature Loop Simulation

The study first tracks how the system reacts when the room temperature is set to 25°C, 20°C or 30°C while the target water temperature remains fixed at 55°C. 25°C is taken as the baseline because it corresponds to the indoor condition generally judged most comfortable for human physiology. The other two levels capture the spread of preferences found in population surveys: 20°C represents occupants who favor cooler surroundings, whereas 30°C covers those who prefer warmer ones. The response curves plotted in Figure 4 almost coincide. Overshoot is 11.46% at 20°C, 11.34% at 25°C and 11.27% at 30°C, a spread of only 0.19%. Rise time is identical at 258s for every case, and settling time differs by less than 1%: 2081s for 20°C and 25°C, 2067s for 30°C.

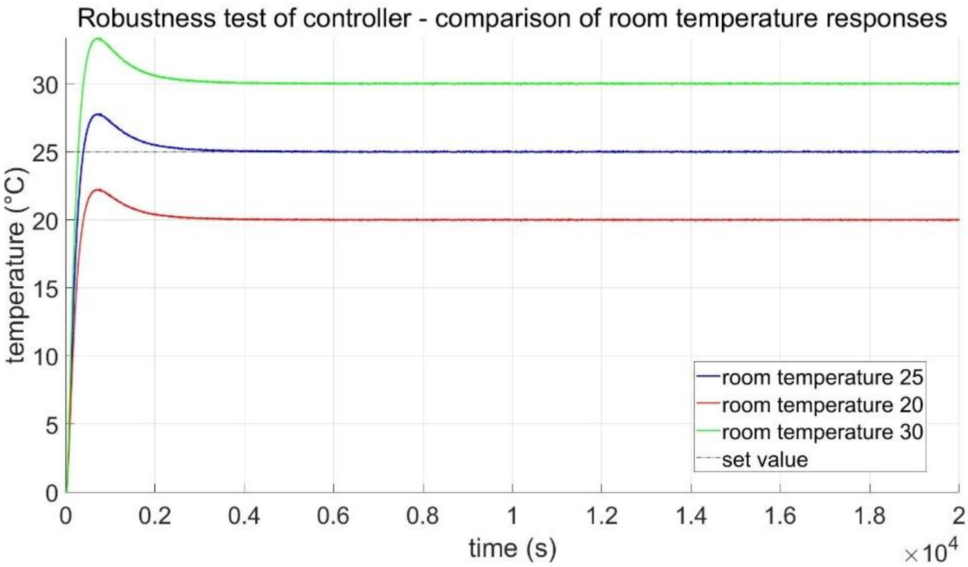

Fig. 4 Comparison of room temperature responses (Picture credit: Original)

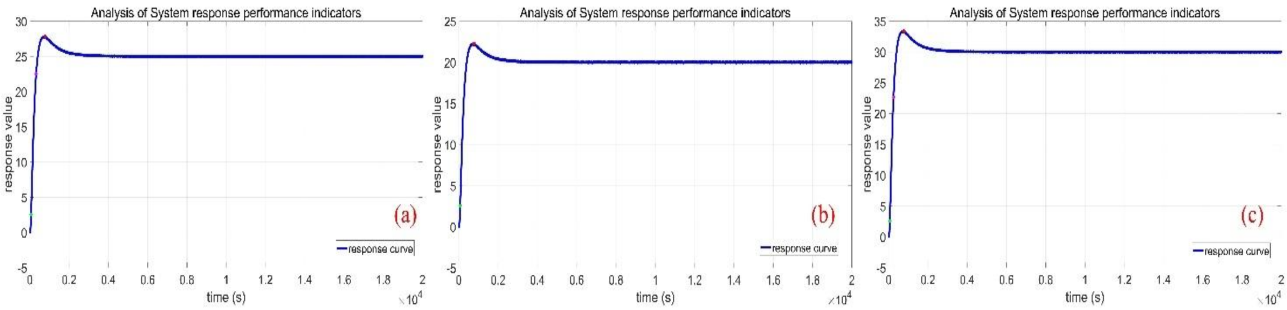

Fig. 5 Dynamic response curves for the room temperature loop at three distinct temperatures. (a) Response curve at 25 degrees. (b) Response curve at 20 degrees (c) Response curve at 30 degrees

Picture credit: Original

Based on Figure 5, calculating the corresponding dynamic characteristic values in Simulink and Table 2 is obtained.

Table 2. Dynamic response data of the room temperature loop

Set temperature(℃)	Peak value(℃)	Overshoot (%)	Rise time (s)	Settling time (±2%)
25	27.8362	11.34	258.00	2081.00
20	22.2928	11.46	258.00	2081.00
30	33.3796	11.27	258.00	2067.00

As Figure 5 and Table 2 show, the room-temperature loop’s dynamic figures stay almost the same no matter how the setpoint is shifted. This matches classical control theory: because the model is linear and time-invariant, the shape of the transient—rise time, damping, and so on—is fixed by the loop transfer function and the constant PID settings. A step in the setpoint therefore produces curves that differ only in height, not in form. The controller thus keeps its behavior uniform and stable across operating points, proving itself robust to its own setpoint changes.

3.2. Analysis of Water Tank Temperature Loop Simulation

This paper sets the target water temperature to 55°C and repeated the test at ambient temperatures of 25°C, 20°C and 30°C. The resulting transient curves, plotted in Figure 6, differ markedly.Overshoot climbs from 11.27% at 30°C to 11.34% at 25°C and 11.46% at 20°C, indicating that hotter surroundings intensify the overshoot. The rise time contracts as room temperature rises (11892s, 995s and 587s) while the settling time stays close to 16000s, shortening only modestly at the highest ambient level.

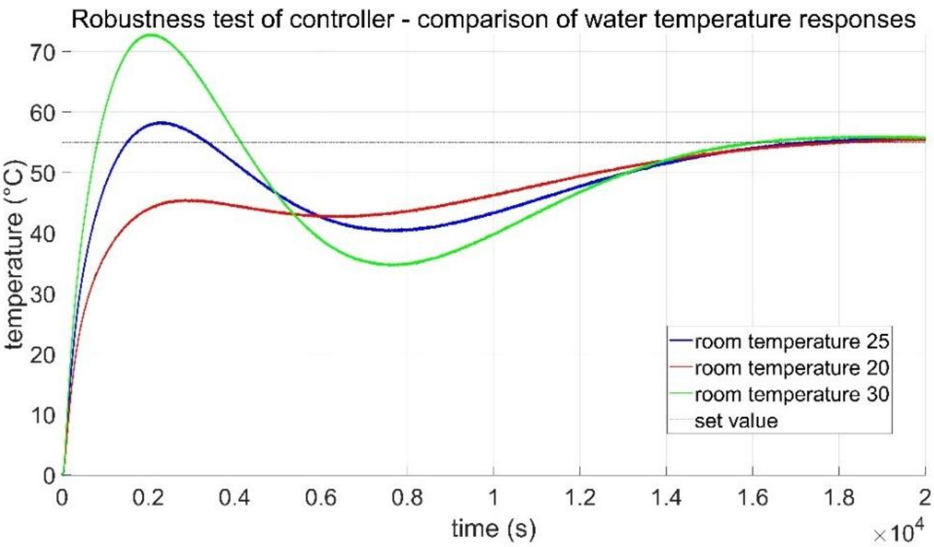

Fig. 6 Comparison of water temperature responses (Picture credit: Original)

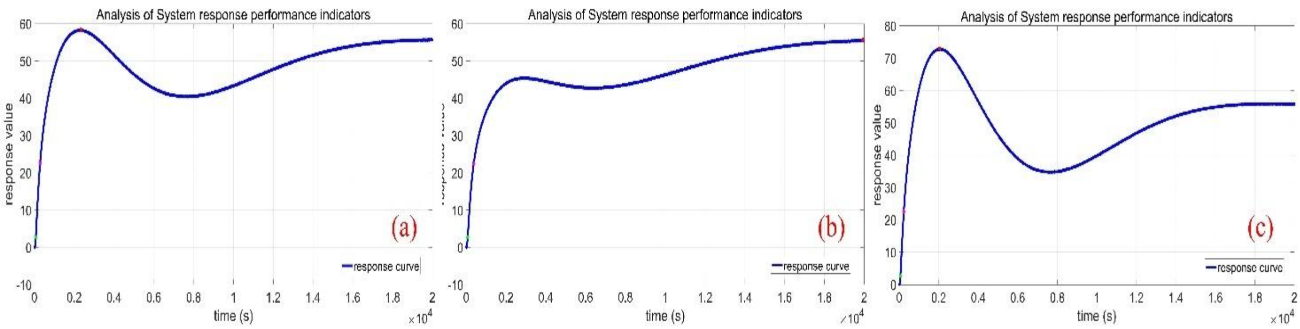

Fig. 7 Dynamic response curves for the water tank temperature loop at three distinct temperatures. (a) Response curve at 25 degrees. (b) Response curve at 20 degrees (c) Response curve at 30 degrees (Picture credit: Original)

Based on Figure 7, calculating the corresponding dynamic characteristic values in Simulink and Table 3 is obtained.

Table 3. Dynamic response data of the water tank temperature loop

Set temperature(℃)	Peak value(℃)	Overshoot (%)	Rise time (s)	Settling time (±2%)
25	58.3626	6.11	995.00	16026.00
20	55.6013	1.09	11892.00	16199.00
30	72.8898	32.53	587.00	15234.00

Figure 7 and Table 3 together show that the two control loops are tightly coupled. The room-temperature set-point fixes how hard the air-conditioning unit runs, and that load fixes the waste-heat power it rejects. This same waste-heat power is the main input that drives the hot-water temperature loop.

Setting the room temperature to 30°C imposes a heavy cooling load on the air-conditioner, forcing it to run at high capacity and discharge a large amount of waste-heat power. This strong thermal input drives the hot-water loop to warm up too rapidly, producing a pronounced overshoot of 32.53% together with sustained oscillations and giving the system an “overdrive” behaviour.

With the room thermostat fixed at 20°C, the cooling demand on the air-conditioning side is modest, so the rejected heat is minimal. The feeble signal sent to the hot-water loop lengthens the warm-up phase to roughly 3.3h and leaves the dynamics sluggish, giving the overall system an under-driven feel.

When the room temperature is set to 25°C (standard value), the system operates under a balanced design condition, achieving relatively stable dynamic performance.

The experiment shows that the hot-water temperature loop behaves quite differently depending on how the room-temperature loop is running. Even though the water-temperature controller settings stay the same, disturbances arriving through the coupling paths reshape the overall plant dynamics and degrade control quality. In other words, under the present architecture the water-temperature controller offers little immunity to coupled disturbances.

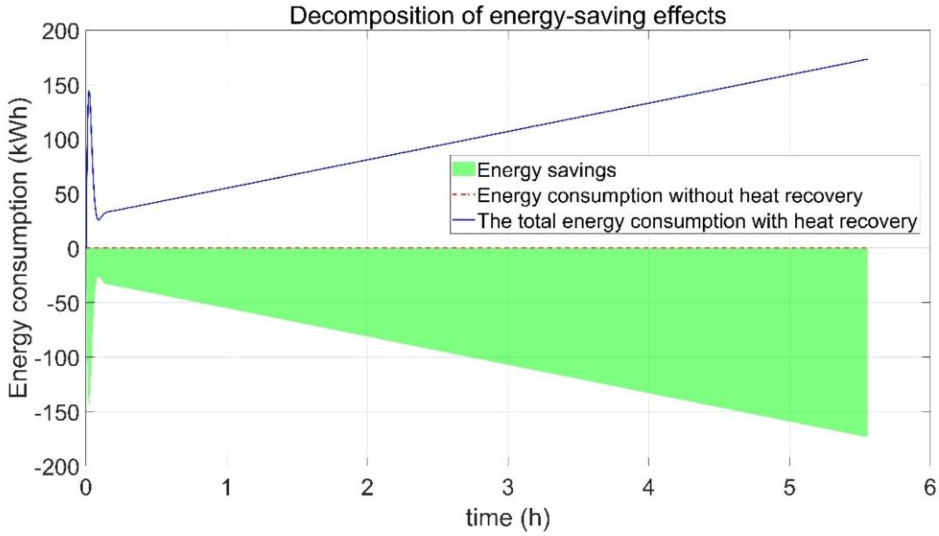

Fig. 8 Decomposition of energy-saving effects (Picture credit: Original)

The decomposition trend shown in the corresponding figure 8 offers clear analytical insight. The green band, which denotes energy savings, is measured as the gap between the cumulative energy-use curves for the case without heat recovery and the case with it. This gap appears at the start of the simulation and widens in an almost straight line, revealing two points: the saving begins the moment cooling and hot-water demand coincide, cutting the electricity that an auxiliary heater would otherwise draw, and it keeps growing as hours of operation accumulate, confirming the long-term value of the heat-recovery measure.

4. Conclusion

Experiments confirm that the integrated energy-recovery unit functions as intended: linking the formerly separate air-conditioning and domestic-hot-water circuits allows the latent heat of condensation to be reclaimed, cutting the combined energy demand. With PID gains left unchanged, the room temperature loop keeps rise time, overshoot and settling period almost constant across set-point adjustments, evidence that the initial tuning is sound and the closed-loop plant is intrinsically stable. The widening gap between the two recorded power traces further quantifies the saving delivered by heat recovery; scavenging waste heat from the air-conditioner to pre-heat service water shortens water heater runtime and lowers its load, raising overall household energy efficiency. Simulations put the whole-house saving at 30%-50%, giving both a technical blueprint and a theoretical basis for curbing residential carbon emissions and shrinking energy bills. The scheme is equally relevant to home equipment coupling and to industrial retrofits, aligning with national conservation targets. Time-of-use tariffs and diverse user habits were not modelled; future work will introduce online optimisation and intelligent scheduling to tailor the strategy to individual lifestyles.

References

[1] S. Sadrizadeh, R. Yao, F. Yuan, H. Awbi, W. Bahnfleth, Y. Bi, G. Cao, C. Croitoru, R. de Dear, F. Haghighat, et al. Indoor air quality and health in schools: A critical review for developing the roadmap for the future school environment. Journal of Building Engineering, 2022, 104908.

[2] K. You, Y. Yu, W. Cai, Z. Liu. The change in temporal trend and spatial distribution of CO2 emissions of China's public and commercial buildings. Build. Environ, 2023, 229, 109956.

[3] Y. Balali, A. Chong, A. Busch, S. O'Keefe. Energy modelling and control of building heating and cooling systems with data-driven and hybrid models—A review. Renew. Sustain. Energy Rev, 2023, 183, 113496.

[4] Yu Sun, Xinyi Zhang, Yongqi Zeng, Yuhang Zhang, Dong Huang, Rijing Zhao. Experimental study on serpentine-looped minichannel pulsating heat pipe heat exchanger with horizontal installation for full-year efficient heat recovery in air conditioning. International Journal of Refrigeration, 2025, 178, 71-87.

[5] H. Willem, Y. Lin, A. Lekov. Review of energy efficiency and system performance of residential heat pump water heaters. Energy and Buildings, 2017, 143, 191-201.

[6] Gleiston Guerrero-Ulloa, Alex Andrango-Catota, Martín Abad-Alay, Miguel J. Hornos, Carlos Rodríguez-Domínguez. Development and assessment of an indoor air quality control IoT-based system. Electronics, 2023, 12(3), 608.

[7] K. Alanne, S. Sierla. An overview of machine learning applications for smart buildings. Sustainable Cities Soc, 2022, 76, 103445.

[8] B. Yu, A.H.C. van Paassen. Simulant and bond graph modeling of an airconditioned room. Simul. Model. Pract, 2004, 12, 61-76.

[9] Jean-Nicolas Louis, Antonio Calo, Kauko Leiviskä, Eva Pongrácz. Environmental Impacts and Benefits of Smart Home Automation: Life Cycle Assessment of Home Energy Management System. IFAC-PapersOnLine, 2015, 48(1), 880-885.

[10] Araújo A, Pereira V. Solar thermal modeling for rapid estimation of auxiliary energy requirements in domestic hot water production: proportional flow rate control. Energy, 2017, 138, 668-681.

[11] Domenico Gorni, María del Mar Castilla, Antonio Visioli. An efficient modelling for temperature control of residential buildings. Building and Environment, 2016, 103, 86-98.

[12] Zhang J, Guo L. PID control of nonlinear stochastic systems with structural uncertainties. IFAC-PapersOnLine, 2020, 53(2), 2189-2194.